# Locally Modified Version of Bott's Advection Scheme

ANDREAS CHLOND

*Max-Planck-Institut für Meteorologie, Hamburg, Germany*

(Manuscript received 15 February 1993, in final form 26 May 1993)

ABSTRACT

A simple and effective self-adjusting hybrid technique has been introduced to develop a new conservative and monotonic advection scheme that exhibits very low numerical diffusion of resolvable scales. The proposed scheme combines Bott's area-preserving flux-form algorithm with an area-preserving exponential interpolating scheme, the use of either at any particular location being automatically controlled by the local ratio of the nodal values involved in the approximation process.

The performance of the combined scheme is illuminated in a series of one- and two-dimensional linear advection experiments. The comparative test calculations presented demonstrate that the combined scheme provides highly accurate solutions both in regions where the transported flow variable is smooth and in the vicinity of sharp gradients. Furthermore, the self-adjusting hybrid technique is highly effective in removing numerical artifacts such as dispersive ripples and simultaneously requires only an admissible additional computational effort relative to Bott's scheme. Thus, it is concluded that the combined scheme is well suited for many atmospheric modeling applications where advection plays a significant role.

## 1. Introduction

Advective processes are of central importance in geophysical fluid dynamics and their treatment is crucial in numerical modeling of the transport of trace constituents in atmospheric models. However, the numerical handling of advection is plagued with difficulties. For instance, problems may arise when the transport of positive-definite scalar quantities, such as moisture, liquid water content, and chemical concentrations, is treated, since unphysically negative constituent values may be generated and/or strong spatial gradients can be smeared out or ripples can be produced in their vicinity by the numerical scheme. Hence, the numerical approximation of advective transport is a classical example of an exercise in compromise, attempting here to reconcile the requirements of stability, accuracy, and algorithmic simplicity. The main conflict arises from the need to retain or introduce some kind of stabilizing diffusive mechanism against the desire to maximize accuracy by minimizing numerically diffusive agencies.

During the past decades, a wide variety of finite-difference methods has been suggested for the numerical solution of the advection equation and several intercomparisons have been published (e.g., see Woodward and Colella 1984; Rood 1987; Müller 1992 for reviews). However, many of these transport schemes do not adequately model the advection equation. For instance, the well-known upstream scheme suffers from high numerical diffusion. The fourth-order-accurate scheme of Crowley (1968) and the third- and higher-order-accurate schemes of Tremback et al. (1987), which use the method of polynomial fitting to represent the local distribution of a dependent variable inside a grid box, are far less diffusive than the upwind approximation, but because of dispersion errors the solutions are not ripple-free, and therefore, these schemes cannot obviate the problem of unphysical negative mixing ratios. Recent advances in numerical techniques designed specifically for meteorological models provided a number of positive-definite schemes (or positive-definite corrections to be applied to existing schemes), that is, schemes that do not allow physically positive quantities to become negative. Smolarkiewicz (1983, 1984) developed a conservative and positive-definite scheme that has found many applications over the last years. He introduced corrective advection fluxes to reduce the truncation error caused by the upstream method. Based on the integrated flux schemes of Tremback et al. (1987), Bott (1989a,b) presented a conservative positive-definite advection algorithm that is computationally very efficient. His procedure consists in the normalization and limitation of the advective fluxes employing specific limiters to avoid negative mixing ratios. Prather's scheme (1986), which is an extension of the slopes scheme of Russel and Lerner (1981), uses a polynomial expression to represent the tracer concentration within each grid box. In his scheme, first-order moments (i.e., slope) as well as sec-

*Corresponding author address:* Dr. Andreas Chlond, Max-Planck-Institut für Meteorologie, Bundestrasse 55, D-2000 Hamburg 13, Germany.

ond-order moments (i.e., curvature) of the distribution are transported in addition to the cell average (i.e., zeroth-order moments) to reduce numerical diffusion. Prather also presents a method to assure sign preservation. However, although these methods work quite well and are widely used in the meteorological community, their applicability is mainly restricted to flows that exhibit comparatively smooth gradients, because they cannot control dispersive ripples. Especially in regions of steep gradients of the transported quantity, these schemes display unphysical oscillations (i.e., the schemes produce over- and undershoots) that can be sufficiently serious to cause numerical instability.

A number of methods have been proposed to suppress these unphysical "wiggles" (see, e.g., Woodward and Colella 1984; Rood 1987), most of which are based on the introduction of artificial diffusion. However, these schemes are highly empirical, relying on experience to determine the level of diffusion coefficients for particular applications to keep the rippling from occurring. Other, more systematic approaches are based on the flux corrected transport (FCT) method of Boris and Book (1973, 1976), Book et al. (1975), and Zalesak (1979). The basic idea of this approach is to blend the results of two difference schemes together. FCT constructs the advective fluxes point by point as weighted averages of a flux computed by a monotonic, but diffusive, low-order scheme and a flux computed by a high-order scheme. The criterion used to control the weighting or blending factors is to ensure that the high-order flux is used to the greatest extent possible without introducing ripples, and this constraint leads to blending factors that depend on local conditions. The principal disadvantage of this flux blending is such, however, that the contribution of the low-order scheme is much greater than needed for avoiding spurious oscillations, especially in regions of steep gradients of the transported quantity. Hence, a certain amount of additional numerical diffusion must be tolerated, which results in smearing out of sharp gradients. Based on the FCT methodology, Smolarkiewicz and Grabowski (1990) and Bott (1992) extended their original positive-definite approach to monotonicity preservation.

A third method, the piecewise parabolic method (PPM) (Colella and Woodward 1984; Woodward 1986; Carpenter et al. 1990), uses cell averages to construct a unique, monotonic parabola that represents the distribution of a dependent variable within a grid box. This scheme is nonoscillatory by construction and thus monotonicity preserving. The principal drawback of this scheme is its complexity and the consequent great computational expense [see article by Müller (1992)].

In this paper we present a monotone version of the area-preserving flux-form advection algorithm of Bott (1989a,b) using a simple but effective switching procedure. In contrast to the approach of Bott (1992), which uses the concept of the FCT method to limit the total advective fluxes, we do not use specific limiters to achieve monotonicity. In principle, our scheme combines Bott's flux scheme with an exponential upstream-weighted interpolation, the use of either at any particular location being essentially controlled by the local ratio of the nodal values involved in the approximation process. Hence, the Bott scheme is used in the bulk of the domain in regions with smooth gradients; when the local curvature of the advected variable exceeds a preset value, however, the algorithm automatically switches to exponential upwinding. Since we use exponential interpolation functions, the scheme is nonoscillatory by construction and the scheme introduces implicitly and locally just enough diffusion into only those regions in which, otherwise, oscillations would occur, and this introduction is automatically controlled through a dynamic adjustment of the switch during the solution process. As a result, the hybrid scheme is also appropriate to address problems with sharp gradients and the scheme produces solutions that are found to be very close to those of the Bott scheme but displaying no over- or undershoots.

The paper is organized as follows. In section 2 we describe the details of the numerical methodology. Numerical results of different advection experiments in one and two spatial dimensions are presented in section 3 to illustrate the performance of the resulting scheme. Finally, the conclusions are summarized in section 4.

## 2. Theory

### *a. The continuity equation*

To illustrate the problem, we consider the continuity equation describing the advection of a nondiffusive quantity in a nondivergent flow field; that is,

$$\frac{\partial \psi}{\partial t} = -\nabla \cdot (\mathbf{v}\psi), \tag{1}$$

where $\psi(\mathbf{x}, t)$ is the nondiffusive scalar quantity, $\mathbf{v} = (u, v, w)$ is the velocity vector, $\mathbf{x} = (x, y, z)$ is the position vector in a Cartesian coordinate system, and $t$ is the time. For simplicity, the proposed numerical solution of (1) will be derived only for the one-dimensional case, namely,

$$\frac{\partial \psi}{\partial t} = -\frac{\partial}{\partial x}(u\psi). \tag{2}$$

With the assumption of a constant positive velocity, (2) represents the shape-conserving movement of an initial distribution toward positive $x$. Since the analytic solution is known in this simple case, the numerical solution can be critically evaluated. A method for performing multidimensional calculations is the technique of directional splitting (Strang 1968; Yanenko 1971). In this technique, a multidimensional problem is solved

by means of successive, one-dimensional sweeps in each of the coordinate directions. In this connection it should be noted that the application of the splitting procedure requires some caution because some schemes lose their accuracy or stability when too simple directional splitting algorithms are used; for example, the decomposition of three-dimensional advection into three separate one-dimensional steps may lead to instability; instead the second-order splitting in three dimensions requires alternating two-dimensional and one-dimensional schemes (Peyret and Taylor 1983). However, it turns out that our scheme takes well to directional splitting, and we conclude that this technique is an efficient method for extending our one-dimensional scheme to two or three dimensions.

Denoting the flux of $\psi$ past the point $x$ at time $t$ with

$$F(x, t) = u\psi, \tag{3}$$

the continuity equation then reads

$$\frac{\partial \psi}{\partial t} = -\frac{\partial}{\partial x} F. \tag{4}$$

To solve (4) a "finite-volume" technique is used that is based on control-volume-averaged data. Hence, the continuity equation (4) is integrated in space from $x - (\Delta x/2)$ to $x + (\Delta x/2)$ and in time from $t$ to $t + \Delta t$ to obtain the control-volume formulation. The mass conservation principle applied to any finite-control volume then reads

$$\langle \psi \rangle_{t+\Delta t} = \langle \psi \rangle_t - \frac{\Delta t}{\Delta x} (\bar{F}_R - \bar{F}_L), \tag{5}$$

where subscripts $L$ and $R$ denote the left and right edges of the associated control volume. Angle brackets denote control-volume averages and an overbar denotes a temporal average, which are given by

$$\langle a \rangle = \frac{1}{\Delta x} \int_{x-(\Delta x/2)}^{x+(\Delta x/2)} a dx$$

$$\bar{a} = \frac{1}{\Delta t} \int_{t}^{t+\Delta t} a dt, \tag{6}$$

where $a$ is any variable, $\Delta x$ is the control volume width, and $\Delta t$ is the time increment.

Thus, the time change of the area average of $\psi$ in the control volume $x - (\Delta x/2) \leq x' \leq x + (\Delta x/2)$ during a time step $\Delta t$ is equal to the amount of constituent transported across the boundaries into or out of the grid volume.

### b. *Bott's flux scheme*

Recently, Bott (1989a,b) presented an upstream-biased Eulerian finite-volume advection scheme conserving mass, being positive definite, and possessing small amplitude and phase errors. To develop the numerical advective operator, Bott uses the methodology of Trembeck et al. (1987). The advection procedure proceeds in two steps. In the first step, area-preserving polynomials are used to calculate the transport fluxes. In the second step, specific limiters are employed to avoid negative mixing ratios.

To derive the method, the calculation domain is divided into a number of nonoverlapping control volumes such that there is one control volume surrounding each grid point. We adopt the notation that subscripts $i$ refer to discrete locations in the $x$ direction with constant grid spacing $\Delta x$, and superscripts $n$ refer to discrete times with time interval $\Delta t$. The discretized form of (5) then reads

$$\psi_i^{n+1} = \psi_i^n - \frac{\Delta t}{\Delta x} [\bar{F}_{i+1/2} - \bar{F}_{i-1/2}], \tag{7}$$

where $\psi_i^n$ is the value of $\psi$ at grid point $i$ after $n$ time steps and $\bar{F}_{i+1/2}$, $\bar{F}_{i-1/2}$ are the time-averaged approximate $\psi$ fluxes through the right and left boundaries of the grid box, respectively. According to (3) and (6), we write $\bar{F}_{i+1/2}$ as follows (assuming constant $u$ for the moment):

$$\bar{F}_{i+1/2} = \frac{1}{\Delta t} \int_0^{\Delta t} [u\hat{\psi}(x, t + t')]_{x=x_i+(\Delta x/2)} dt'$$

$$= \frac{1}{\Delta t} \int_0^{\Delta t} [u\hat{\psi}(x - ut', t)]_{x=x_i+(\Delta x/2)} dt' \tag{8}$$

where $\hat{\psi}(x, t)$ denotes a piecewise profile representing the variation of $\psi$ between the grid points. With $x' = x - ut'$, (8) becomes

$$\bar{F}_{i+1/2} = \frac{1}{\Delta t} \int_{x_{i+1/2}-u\Delta t}^{x_{i+1/2}} \hat{\psi}(x', t) dx'. \tag{9}$$

Hence, the advective flux is proportional to the total mass of constituent transported through the right boundary of the grid box $i$ during the time interval $\Delta t$, which corresponds to the integral of $\hat{\psi}(x', t)$ extending from a point at a distance $u\Delta t$ upwind of $x_{i+1/2}$ to $x_{i+1/2}$. Relaxing the condition of constant $u$ and using the notations

$$x''(i) = \frac{x' - x_i}{\Delta x}, \quad C_{i+1/2}^{n+} = \max\left(O, \frac{u_{i+1/2}^n \Delta t}{\Delta x}\right)$$

and

$$C_{i+1/2}^{n-} = -\min\left(O, \frac{u_{i+1/2}^n \Delta t}{\Delta x}\right),$$

(9) could be written

$$\bar{F}_{i+1/2} = \frac{\Delta x}{\Delta t} (I_{i+1/2}^+ - I_{i+1/2}^-), \tag{10}$$

where

$$I^{+}_{i+1/2} = \int_{1/2-C^{n+}_{i+1/2}}^{1/2} \hat{\psi}[x''(i), t]\, dx''(i)$$

$$I^{-}_{i+1/2} = \int_{-1/2}^{-1/2+C^{n-}_{i+1/2}} \hat{\psi}[x''(i+1), t]\, dx''(i+1). \tag{11}$$

To evaluate the integrals in (11), Bott (1989a,b) applied the polynomial fit methodology developed by Crowley (1968) and Tremback et al. (1987). In this way, the local $\psi$ distribution inside a grid box $i$ is represented using an area-preserving polynomial of order 1:

$$\hat{\psi}(x'(i), t) = \psi^n_{i,l}[x'(i)] = \sum_{k=0}^{l} a^n_{i,k} x'^k(i). \tag{12}$$

The coefficients $a^n_{i,k}$ are functions of the $\psi$ values at grid point $i$ and at neighboring grid points $i \pm 1, \ldots, i \pm l/2$ and are determined from the requirements that at $x_{i\pm1}, \ldots, x_{i\pm l/2}$ the values of $\psi^n_{i,l}[x'(i)]$ agree with $\psi^n_{i\pm1}, \ldots, \psi^n_{i\pm l/2}$ and that the area covered by $\psi^n_{i,l}[x'(i)]$ in grid box $i$ equals $\psi^n_i \Delta x$. Table 1 lists values of $a^n_{i,k}$ for $l = 2$ and $l = 4$ (after Bott 1989b). Substitution of (12) into (11) yields the integrals $I^{+}_{i\pm1/2}$ and $I^{-}_{i+1/2}$, respectively (superscript $n$ omitted):

$$I^{+}_{i+1/2,l} = \sum_{k=0}^{l} \frac{a_{i,k}}{(k+1)2^{k+1}} [1 - (1 - 2C^{+}_{i+1/2})^{k+1}]$$

$$I^{-}_{i+1/2,l} = \sum_{k=0}^{l} \frac{a_{i+1,k}}{(k+1)2^{k+1}} \times (-1)^k [1 - (1 - 2C^{-}_{i+1/2})^{k+1}]. \tag{13}$$

Finally, positive definiteness of the scheme is obtained in two steps by introducing the following nonlinear flux limiters. First, the flux $\bar{F}_{i+1/2}$ should have the same sign as the advecting velocity $u_{i+1/2}$; otherwise, it will be put to zero. Second, the flux $\bar{F}_{i+1/2}$ is limited in such a way that the total amount of outflux from a grid box $i$ during a time step $\Delta t$ is limited by $\psi^n_i \Delta x/\Delta t$. Combining these restrictions, the flux $\bar{F}_{i+1/2}$ can be written in the form

$$\bar{F}_{i+1/2} = \frac{\Delta x}{\Delta t} (\beta_{i+1/2} \tilde{I}^{+}_{i+1/2,l} - \beta_{i+3/2} \tilde{I}^{-}_{i+1/2,l}), \tag{14}$$

with

$$\tilde{I}^{+}_{i+1/2,l} = \max(I^{+}_{i+1/2,l}, 0)$$

$$\tilde{I}^{-}_{i+1/2,l} = \max(I^{-}_{i+1/2,l}, 0)$$

$$\beta_{i+1/2} = \min[1, \psi^n_i / \max(\tilde{I}^{+}_{i+1/2,l} + \tilde{I}^{-}_{i-1/2,l}, \epsilon)], \tag{15}$$

where $\epsilon$ is a small value—for example, approximately $10^{-15}$—which has been introduced to avoid the numerical unstable situation with $\tilde{I}^{+}_{i+1/2,l} + \tilde{I}^{-}_{i-1/2,l} = 0$. Similar equations for $\bar{F}_{i-1/2}$ are obtained by replacing $i$ with $i - 1$ in the preceding equations. For a more detailed description and discussion of the scheme and the flux limitation, the reader is referred to the original papers of Bott (1989a,b).

### c. *The exponential upwind scheme*

The exponential upwinding interpolation concept is based on previous work of Spalding (1972). In this approach, piecewise exponential profiles are used to express the variation of $\psi$ between the grid points. The exponential interpolation function in grid box $i$ may be uniquely described by three coefficients ($A^n_i$, $B^n_i$, $D^n_i$) of the following equation:

$$\hat{\psi}[x'(i), t] = \psi^n_{i,E}[x'(i)] = A^n_i + B^n_i \exp[D^n_i x'(i)], \tag{16}$$

where $x'(i)$ is again a normalized grid coordinate. To determine the coefficients $A^n_i$, $B^n_i$, and $D^n_i$, infor-

TABLE 1. Coefficients $a_{i,k}$ for the $l = 2$ and $l = 4$ versions of Bott's area-preserving flux-form algorithm (after Bott 1989b).

| | $l = 2$ | $l = 4$ |
|---|---|---|
| $a_{i,0}$ | $-\frac{1}{24}(\psi_{i+1} - 26\psi_i + \psi_{i-1})$ | $\frac{1}{1920}(9\psi_{i+2} - 116\psi_{i+1} + 2134\psi_i - 116\psi_{i-1} + 9\psi_{i-2})$ |
| $a_{i,1}$ | $\frac{1}{2}(\psi_{i+1} - \psi_{i-1})$ | $\frac{1}{48}(-5\psi_{i+2} + 34\psi_{i+1} - 34\psi_{i-1} + 5\psi_{i-2})$ |
| $a_{i,2}$ | $\frac{1}{2}(\psi_{i+1} - 2\psi_i + \psi_{i-1})$ | $\frac{1}{48}(-3\psi_{i+2} + 36\psi_{i+1} - 66\psi_i + 36\psi_{i-1} - 3\psi_{i-2})$ |
| $a_{i,3}$ | — | $\frac{1}{12}(\psi_{i+2} - 2\psi_{i+1} + 2\psi_{i-1} - \psi_{i-2})$ |
| $a_{i,4}$ | — | $\frac{1}{12}(\psi_{i+2} - 4\psi_{i+1} + 6\psi_i - 4\psi_{i-1} + \psi_{i-2})$ |

mation from grid point $i$ and two neighboring grid points is used demanding that at $x_{i\pm1}$ the values of $\psi^n_{i,E}[x'(i)]$ agree with $\psi^n_{i\pm1}$ and that the integrated area beneath each interpolation curve is preserved. Thus, the resulting set of defining equations will be (superscripts $n$ omitted henceforth except where confusion is possible)

$$\psi_{i-1} = A_i + B_i \exp(-D_i) \tag{17a}$$

$$\psi_i = A_i + \frac{B_i}{D_i}\left[\exp\left(\frac{D_i}{2}\right) - \exp\left(-\frac{D_i}{2}\right)\right] \tag{17b}$$

$$\psi_{i+1} = A_i + B_i \exp(D_i). \tag{17c}$$

Combining (17a) and (17c) yields

$$A_i = \psi_{i-1} - \frac{(\psi_{i+1} - \psi_{i-1})\exp(-D_i)}{\exp(D_i) - \exp(-D_i)} \tag{18a}$$

$$B_i = \frac{\psi_{i+1} - \psi_{i-1}}{\exp(D_i) - \exp(-D_i)}. \tag{18b}$$

The substitution of (18a) and (18b) into (17b) leads to a nonlinear equation for $D_i$,

$$\left[\frac{\psi_i - \psi_{i-1}}{\psi_{i+1} - \psi_{i-1}} + \frac{\exp(-D_i)}{\exp(D_i) - \exp(-D_i)}\right]D_i - \frac{\exp(D_i/2) - \exp(-D_i/2)}{\exp(D_i) - \exp(-D_i)} = 0. \tag{18c}$$

which can be solved easily using Newton's method. In this manner, the coefficients $A_i$, $B_i$, and $D_i$ of the interpolation curve may be obtained from (18c), (18a), and (18b). Finally, substitution of (16) into (11) yields the integrals $I^+_{i+1/2}$ and $I^-_{i+1/2}$, respectively:

$$I^+_{i+1/2,E} = A_i C^+_{i+1/2} + \frac{B_i}{D_i} \times \left\{\exp\left(\frac{D_i}{2}\right) - \exp\left[\frac{D_i}{2}(1 - 2C^+_{i+1/2})\right]\right\}$$

$$I^-_{i+1/2,E} = A_{i+1} C^-_{i+1/2} + \frac{B_{i+1}}{D_{i+1}}\left\{\exp\left(-\frac{D_{i+1}}{2} \times \left[1 - 2C^-_{i+1/2}\right]\right) - \exp\left(-\frac{D_{i+1}}{2}\right)\right\}. \tag{19}$$

It is important to note that due to the local exponential curve-fitting procedure the advection algorithm in this form is well suited for accurately representing sharp gradients. Since the interpolation formula is monotonic by construction, the advection procedure ensures (especially in the vicinity of localized sharp interfaces) that positive quantities will remain positive and that sharp gradients will be handled correctly without the generation of spurious oscillations. The main disadvantages of the exponential scheme relate to the high computational costs associated with the solution of (18a)–(18c) and with the evaluation of (19). Moreover, since the exponential fitting procedure is possible only (and therefore available) in the monotonic regime of the flow, the question remains as to the best procedure to treat nonmonotonic regimes (i.e., local extrema of the advected variable). A simple and apparently robust strategy is to use the ordinary first-order upwinding scheme for the case that the zone average of the advected variable is a local extremum. However, this procedure adds a substantial amount of numerical diffusion to the scheme so that the exclusive use of the pure exponential scheme cannot be recommended even if computer costs were not an issue. (See also section 3a, where we present results using only the exponential scheme.) The "automatic switch" described in the next section has therefore been designed in a way to adequately check for these regions.

### *d. The combined scheme*

As already stated in section 2b, Bott's flux scheme has several attractive properties: the method is mass conservative and positive definite, has small phase and amplitude errors, and is computationally very efficient. However, the simulation of sharply varying gradients—especially in situations with nonzero background values of the transported quantity—can result in unphysical oscillations, which although localized could cause difficulties in nonlinear problems.

To eliminate this deficiency of the scheme and to ensure monotonicity, we use a variant of Harten and Zwas's (1972) self-adjusting hybrid technique. The basic idea is to identify regions where monotonicity might be violated and then keep the rippling from occurring. This goal is achieved by combining Bott's accurate scheme, which is used in the smooth regions of the transported quantity, with the exponential scheme that is used in regions of sharp gradients. (Hence, the name "hybrid" is indicative of a combination of two different methods.) The use of either of these two schemes at any particular location is controlled by a switch that automatically (i.e., self-adjusting) switches from one scheme to the other. Since the exponential interpolation functions are monotonic by construction, no specific flux limiters have to be employed to avoid spurious oscillations near sharp gradients. Thus, we propose to construct the hybrid scheme using a combination of the unlimited Bott scheme and the exponential scheme. Formally, we write the advective $\psi$ flux through the right boundary of the grid box $i$ as follows:

$$\bar{F}_{i+1/2} = \frac{\Delta x}{\Delta t}[(1 - S_i)I^+_{i+1/2,I} + S_i I^+_{i+1/2,E} - (1 - S_{i+1})I^-_{i+1/2,I} - S_{i+1}I^-_{i+1/2,E}], \tag{20}$$

where $I^\pm_{i+1/2,I}$ and $I^\pm_{i+1/2,E}$ denote the area integrals obtained using the polynomial- and exponential-fitting techniques, respectively, defined in (13) and (19). The dimensionless quantity $S_i$, which will be called the

"automatic switch," admits only two states and should have the property

$$S_i = \begin{cases} 1, & \text{in "danger zones"} \\ 0, & \text{in "smooth zones"} \end{cases}. \tag{21}$$

To identify the "danger zones" where monotonicity might be violated we introduce the so-called "monitor functions" $m_i^{(1)}$, $m_i^{(2)}$, and $m_i^{(3)}$ defined by

$$\begin{aligned} m_i^{(1)} &= \frac{|\psi_{i+1} - 2\psi_i + \psi_{i-1}|}{|\psi_{i+1} - \psi_{i-1} + \epsilon|} \\ m_i^{(2)} &= \frac{|a_{i,1}^{l=4} - a_{i,1}^{l=2}|}{0.5\,|a_{i,1}^{l=4} + a_{i,1}^{l=2}|} \\ m_i^{(3)} &= \frac{|a_{i,2}^{l=4} - a_{i,2}^{l=2}|}{0.5\,|a_{i,2}^{l=4} + a_{i,2}^{l=2}|}, \end{aligned} \tag{22}$$

where $\epsilon$ is a small number—for example, approximately $10^{-15}$—and $a_{i,1}^{l=4}$, $a_{i,2}^{l=4}$, $a_{i,1}^{l=2}$, $a_{i,2}^{l=2}$ denote the coefficients $a_{i,k}$ for the polynomials of order $l = 2$ and $l = 4$ of Bott's area-preserving flux-form scheme listed in Table 1. Hence, the monitor function $m_i^{(1)}$ measures the local curvature of the advected variable, and the monitor functions $m_i^{(2)}$ and $m_i^{(3)}$ are quantities that, in some way, give a rough estimate of the local spatial truncation error.

For convenience, two additional switches, $S_i^{(1)}$ and $S_i^{(2)}$, are defined:

$$\begin{aligned} S_i^{(1)} &= \begin{cases} 1, \text{ if } \{[t_i^{(\perp)} \leqslant m_i^{(\perp)} \leqslant 1] \text{ and} \\ \quad \{[m_{i-1}^{(\perp)} \leqslant 1] \text{ and } [m_{i+1}^{(\perp)} \leqslant 1]\}\} \text{ or} \\ \quad \{[m_{i-1}^{(\perp)} = 1] \text{ or } [m_{i+1}^{(\perp)} = 1] \text{ or } [m_{i+1}^{(\perp)} = 1]\} \\ 0, \quad \text{otherwise} \end{cases} \\ S_i^{(2)} &= \begin{cases} 1, & \text{if } [m_i^{(2)} \geqslant t_i^{(2)}] \quad \text{or} \quad [m_i^{(3)} \geqslant t_i^{(2)}], \\ 0, & \text{otherwise} \end{cases} \end{aligned} \tag{23}$$

which are combined according to a logical "OR" to yield the automatic switch $S_i$, such as

$$S_i = \frac{S_i^{(1)} + S_i^{(2)}}{\max[S_i^{(1)} + S_i^{(2)}, 1]}, \tag{24}$$

which constitutes the modification criterion for deciding whether to use Bott's scheme or the exponential upwinding scheme. Here, according to (23) and (24), this nonlinear switch satisfies the conditions imposed by (21); $S_i$ equals zero in regions with smooth varying gradients across a nodal point (this will account for the bulk of the flow field) but equals one in regions where localized sharp transitions are found. Finally, it is important to note that we have coded the exponential upwinding scheme in such a way that it degenerates into an ordinary first-order upwinding scheme in nonmonotonic regimes [i.e., for $m_i^{(1)} > 1$], so that the formulation given by (20) is valid for any arbitrary grid point in the computational domain.

In (23), $t_i^{(1)}$ and $t_i^{(2)}$ are threshold values for which we have chosen

$$\begin{aligned} t_i^{(1)} &= 0.35 \\ t_i^{(2)} &= \begin{cases} 0.35, & \text{if } m_i^{(1)} \leqslant 1 \\ 0.12, & \text{if } m_i^{(1)} > 1 \end{cases}, \end{aligned} \tag{25}$$

which are found to be optimal in the sense that the combined scheme adds implicitly and locally just enough diffusion to suppress unphysical "wiggles." The empirical determination of the coefficients $t^{(1)}$ and $t^{(2)}$ may appear to be a weak point of the method because their determination is based only on a finite number of test functions. To examine the dependence of the numerical solutions on these coefficients, calculations have been performed in which we have varied the threshold values $t^{(1)}$ and $t^{(2)}$ by ±30% around their reference values. This sensitivity study indicates that the combined scheme responds insensitively to variations in these coefficients and that the combined scheme returns in these cases solutions, which are virtually as good as those obtained with the reference values. Therefore, our calculations give grounds for believing that the optimal coefficients given in (25) are of general applicability.

The results of the numerical advection experiments presented in section 3 are obtained using Bott's scheme in the version $l = 4$, abbreviated. The method to use the abbreviated form of Bott's scheme was proposed by Müller (1992). This technique requires that one construct a fourth-order polynomial to provide a local representation of the dependent variable within a grid box. However, only coefficients of the polynomial up to order 2 are used for actually computing the fluxes. In this way the computational effort can be reduced significantly even though the results are quite similar compared to order 4 fitting (Müller 1992).

The extension of the one-dimensional scheme to two dimensions is done with the directional splitting technique (Strang 1968), which requires that one make a series of one-dimensional calculations in the different coordinate directions. Hence, a two-dimensional time step of length $\Delta t$ consists of a sequence of four one-dimensional advection substeps, each of length $\Delta t/2$. To make the calculation symmetrical with respect to $x$ and $y$, a $x$–$y$–$y$–$x$ sequence of sweeps is performed, each one using the output of the previous sweep as input data. Finally, we note that in the deformational flow field test with

$$\frac{\partial u}{\partial x} = -\frac{\partial v}{\partial y} \neq 0$$

(section 3c) we take into account the effects of compressions and rarefractions, which occur during the one-dimensional advection substeps. In this way we improve the accuracy of the directional splitting approach considerably, especially in situations with nonzero background values of the transported quantity.

## 3. Numerical results

In this section numerical results will be presented to examine the performance of the newly proposed combined flux scheme algorithm. The results obtained with the combined scheme will be compared with Bott's (1989a,b) scheme (version $l = 4$, abbreviated) and with the exponential scheme, which will serve as references.

### *a. One-dimensional experiments*

We first consider one-dimensional advection in a constant velocity field. The calculations are performed in a 64-point periodic domain with $\Delta x = 1$. The four types of test problems that are used to evaluate the accuracy of a numerical scheme are the Gaussian function, the square wave function, the triangular function, and the ramp function, which are superimposed on a constant background value of $\psi_B = 100$. Each of these functions helps to illustrate some strengths and limitations of a numerical method. The numerical results presented herein are obtained with constant Courant numbers $C = u\Delta t/\Delta x$ of $C = 0.1$, $C = 0.4$, and $C = 0.8$ after $N_T = 1920$, $N_T = 480$, and $N_T = 240$ iterations, respectively, corresponding to three revolutions around the 64-point periodic domain. As a measure for the total error of a numerical method we use the so-called area ratio (AR), which is the ratio of the total area of the deviations from the exact solution, and the total area and is given by

$$\text{area ratio} = \frac{\sum_i |\psi_i^{N_T} - \psi_i^0|}{\sum_i |\psi_i^0 - \psi_B|}, \qquad (26)$$

where the summation is made over all grid points; $\psi_i^0$ and $\psi_i^{N_T}$ are the values of $\psi$ at grid box $i$ at initial time and after $n = N_T$ time steps (i.e., after three revolutions), respectively. The constant background value is denoted by $\psi_B$. This measure of accuracy turns out to be very useful because the AR gives an estimate of the shape preservation of the numerical solution.

Figure 1 depicts the analytical solution as well as the numerical results of the advection of a Gaussian distribution, which are obtained with (a) Bott's scheme, (b) the exponential scheme, and (c) the combined scheme. (Background values have been removed in this figure and in the following.) For the combined scheme tests, one piece of additional information is included in this and in the following figures: diamonds on the abscissa mark those points at which the "automatic switch" detects a "danger zone" and hence at which the exponential scheme has been activated. Obviously, Bott's scheme and the combined scheme yield a good agreement with the analytical solution and produce low amplitude and phase errors. Thus, this experiment provides a demonstration of each scheme's ability to transport well-resolved, smoothly varying

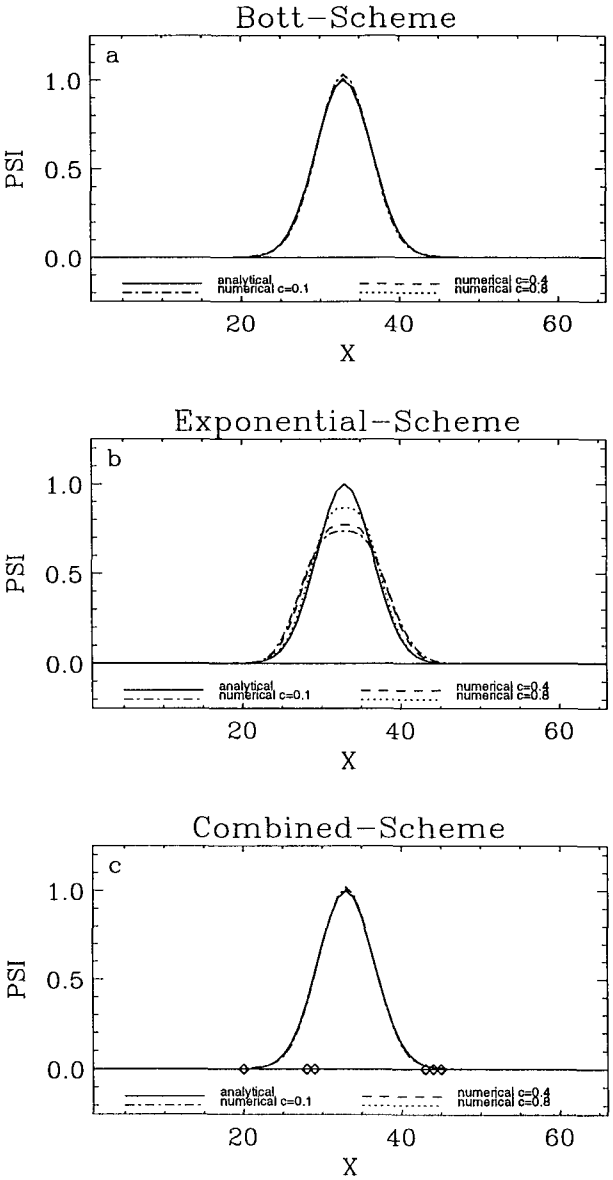


FIG. 1. Solution of the one-dimensional linear advection equation in which a Gaussian distribution superimposed upon a constant background field of $\psi_B = 100$ is advected to the right in a 64-point grid with periodic boundaries. Shown are the analytical solution (full line) along with numerical solutions (dashed lines) obtained (a) with Bott's flux scheme (version $l = 4$, abbreviated), (b) with the exponential scheme, and (c) the combined flux scheme after three revolutions for Courant numbers $C = 0.8$, $C = 0.4$, and $C = 0.1$, corresponding to 240, 480, and 1920 time steps, respectively. The background field has been removed. Diamonds on the abscissa in (c) mark those points at which the exponential scheme has been activated.

functions over large distances. In contrast, the exponential scheme is slightly diffusive and slowly diminishes the amplitude of the Gaussian distribution.

The second example is the advection of the square wave function. This function reveals a numerical method's capability to handle Gibb's oscillations that arise in the vicinity of discontinuities. As shown in Fig. 2a, Bott's scheme generates dispersive ripples that distort the distribution. The exponential scheme (Fig. 2b) broadens the distribution but as a result of monotonicity, exhibits no spurious oscillations; that is, it generates diffusive rather than dispersive errors. The combined scheme, which has activated the exponential interpolation only in the vicinity of the points of discontinuity of the square wave function, produces the best results because it is considerably less diffusive than the exponential scheme and, moreover, it does not introduce wiggles.

The third test is the advection of a triangular distribution that should illustrate a numerical method's capacity to treat sharp peaks and extremum points. As is seen in Fig. 3a, Bott's scheme performs quite well. Dispersive errors are still present but are much smaller in amplitude than for the case of the square wave. Again, the exponential scheme (Fig. 3b) broadens the distribution somewhat but otherwise advects it quite accurately. In Fig. 3c the same problem has been solved using the combined scheme. In this situation, no phase errors and dispersive ripples are visible and the numerical solution is almost identical to the exact solution, except at the lower corner points and in the vicinity of the extremum.

In the final example of one-dimensional advection, a ramplike distribution is transported three revolutions around the 64-point periodic domain. This experiment gives information about each scheme's capability to handle asymmetric functions. As in the case of the square wave function, Bott's algorithm (Fig. 4a) provokes tremendous dispersive ripples in regions with strong spatial gradients of the transported quantity. In contrast, the solution obtained with the combined scheme remains free of spurious oscillations (Fig. 4c). The slope of the ramp function is well represented in regions where the function is only smoothly varying, but the combined scheme tends to broaden the distribution in the vicinity of the localized sharp transition zone by spreading the gradient over several grid boxes. Similarly, the solutions of the exponential scheme (Fig. 4b) are both monotonic and free of spurious oscillations but considerably more diffusive than the combined scheme, spreading the gradient over about ten grid boxes.

The accuracies in terms of the AR for Bott's flux scheme, the exponential scheme, and the combined flux scheme for the four test functions and for various Courant numbers are listed in Table 2. It appears that Bott's scheme and the combined scheme exhibit errors of nearly the same order of magnitude with area ratios

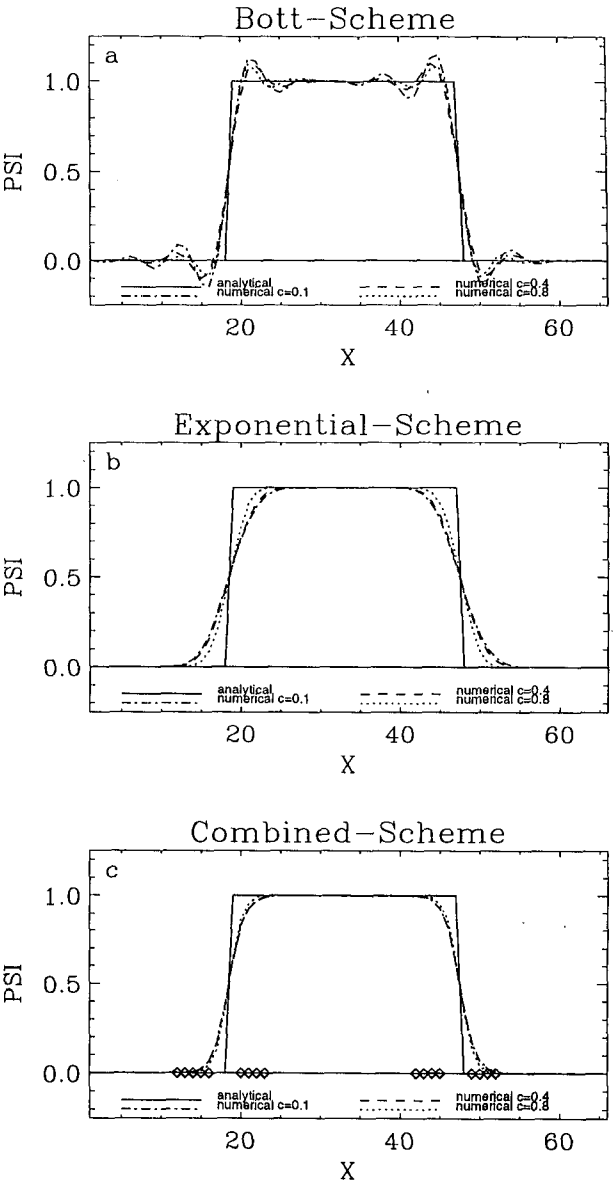


FIG. 2. As in Fig. 1 except for the square wave.

in the range of 0.01–0.12. However, as already stated, Bott's scheme produces mainly dispersion errors that lead to a lack of monotonicity and that can severely distort the distribution, especially in flows where strong gradients or shocks develop. In contrast, as a consequence of the monotonicity constraint, the solutions of the combined scheme are free from Gibb's oscillations, and this scheme generates only small diffusive errors. As a result, the combined scheme produces solutions that are found to be very close to those of Bott's scheme but displaying no over- or undershoots. The exponential scheme produces errors that are at least by a factor of 2 larger than those of Bott's scheme and of the combined scheme. This is certainly not satisfac-

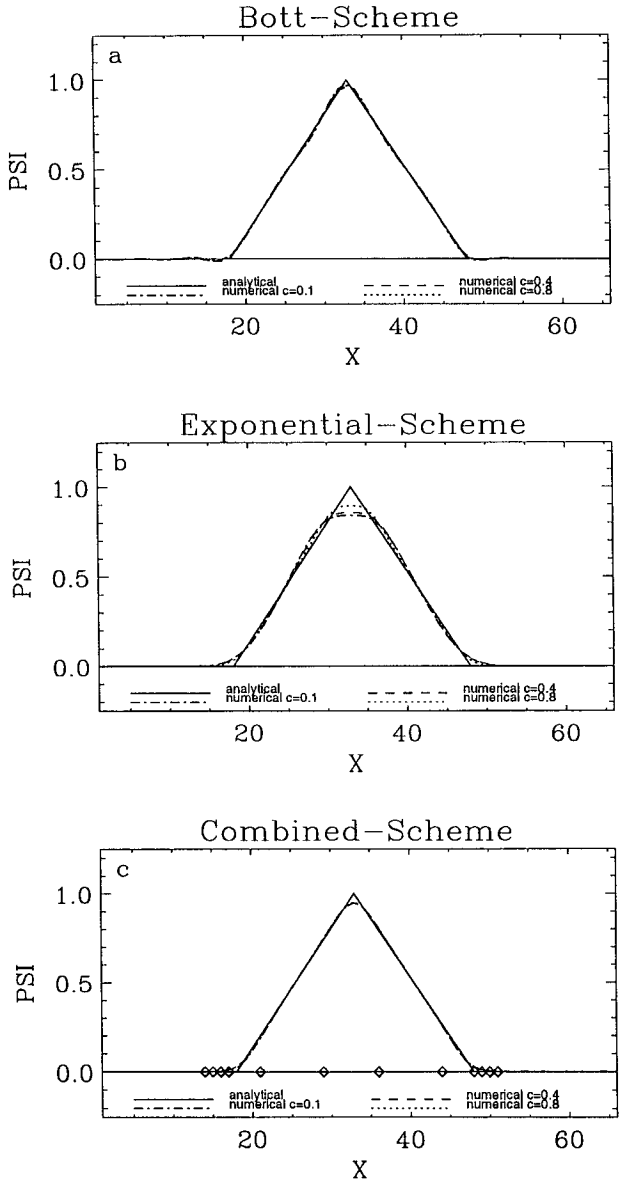


FIG. 3. As in Fig. 1 except for a triangular wave.

tory and indicates, as already stated in section 2c, that the exclusive use of the exponential scheme cannot be recommended.

Finally, we note that our results clearly demonstrate that a positive-definite constraint is less stringent than monotonicity. Moreover, in the case of nonzero background values of the transported quantity, it turns out that Bott's flux limiters are almost inactive. The reason for this is that the limiter is specifically constructed to eliminate negative values of the transported quantity by demanding that the total amount of outflux from a grid box $i$ during a time step is limited by the available amount of $\psi$ in grid box $i$ at time $n$. Hence, in the case of zero background values, the scheme performs quite well by simply cutting away negative values, while in the case of nonzero background values, the procedure fails to work and the limiter therefore additionally allows the generation of new extrema around the level of the background value.

### *b. Two-dimensional rotational flow field test*

In this section we present results of several two-dimensional rotational flow field tests identical to those reported by Smolarkiewicz (1982), in which a prescribed distribution undergoes solid-body rotation counterclockwise around a 100 × 100 zone grid with $\Delta x = \Delta y = 1$. The velocity field is given by

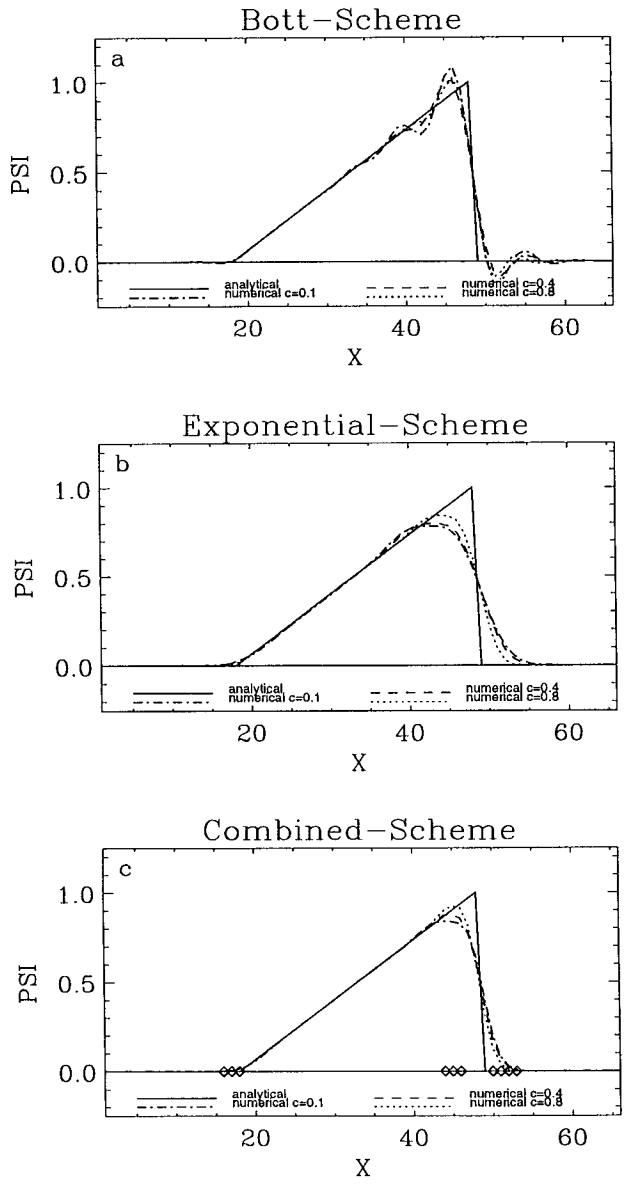


FIG. 4. As in Fig. 1 except for a ramp function.

TABLE 2. Area ratios for Bott's flux scheme, the exponential scheme, and the combined flux scheme after three revolutions around the 64-point periodic domain for various Courant numbers.

| | Area ratios | | | |
|---|---|---|---|---|
| Numerical method | Gauss | Square | Triangle | Ramp |
| Bott ($C = 0.1$) | $3.63 \times 10^{-2}$ | $1.194 \times 10^{-1}$ | $2.82 \times 10^{-2}$ | $1.195 \times 10^{-1}$ |
| Exponential ($C = 0.1$) | $2.424 \times 10^{-1}$ | $1.505 \times 10^{-1}$ | $7.93 \times 10^{-2}$ | $1.757 \times 10^{-1}$ |
| Combined ($C = 0.1$) | $2.15 \times 10^{-2}$ | $9.23 \times 10^{-2}$ | $2.48 \times 10^{-2}$ | $1.038 \times 10^{-1}$ |
| Bott ($C = 0.4$) | $1.42 \times 10^{-2}$ | $1.018 \times 10^{-1}$ | $2.13 \times 10^{-2}$ | $9.99 \times 10^{-2}$ |
| Exponential ($C = 0.4$) | $1.863 \times 10^{-1}$ | $1.367 \times 10^{-1}$ | $7.07 \times 10^{-2}$ | $1.548 \times 10^{-1}$ |
| Combined ($C = 0.4$) | $9.47 \times 10^{-3}$ | $9.06 \times 10^{-2}$ | $2.15 \times 10^{-2}$ | $9.23 \times 10^{-2}$ |
| Bott ($C = 0.8$) | $5.88 \times 10^{-3}$ | $7.97 \times 10^{-2}$ | $1.47 \times 10^{-2}$ | $7.78 \times 10^{-2}$ |
| Exponential ($C = 0.8$) | $8.94 \times 10^{-2}$ | $1.015 \times 10^{-1}$ | $4.45 \times 10^{-2}$ | $1.121 \times 10^{-1}$ |
| Combined ($C = 0.8$) | $7.91 \times 10^{-3}$ | $7.64 \times 10^{-2}$ | $2.09 \times 10^{-2}$ | $7.89 \times 10^{-2}$ |

$$\mathbf{v} = \boldsymbol{\Omega} \times (\mathbf{r} - \mathbf{r}_0), \tag{27}$$

with a constant angular velocity of $|\boldsymbol{\Omega}| = 0.1\ \mathrm{s}^{-1}$ and a rotation center located at $\mathbf{r}_0 = (50, 50)$. The integrations are carried out with a time step of $\Delta t = 0.1$, so that 628 time steps will effect one complete revolution about the central point. The maximum Courant number in the domain is 0.7. As initial conditions we use three different test functions: the cone, the cube, and the grooved cylinder, which are superimposed upon a constant background value of $\psi_B = 100$.

In the first experiment the cone is initialized with a base radius of $15\Delta x$ and a maximum height of $\psi_{\max} = 3.87$ at $(x, y) = (50, 75)$. Figure 5 shows (a) the initial distribution and (b) the final distribution after six full rotations (3768 time steps) obtained with Bott's flux scheme (c) and with the combined flux scheme. As expected, both schemes exhibit very good shape-preserving characteristics. Bott's scheme leaves the maximum amplitude of the cone nearly unchanged but creates new extrema in the distribution at the base of the cone. In contrast, the combined scheme produces no over- or undershootings but reduces the maximum slightly with $\psi^n_{\max}$, finally reaching 93.5% of $\psi^0_{\max}$.

A more severe test problem is the rotation of a cube of unit height with lateral lengths of $20\Delta x$ centered at $(x, y) = (30, 70)$, (see Fig. 6a). Figure 6 presents a comparison of the results of the two schemes for six full rotations of the cube. Bott's scheme generates dispersive errors that severely distort the distribution. In contrast, the combined scheme preserves the shape of the cube very well but tends to broaden the distribution somewhat. However, no oscillations occur either at the base or at the top of the cube.

The last calculation is performed with a rather severe test function similar to that proposed by Zalesak (1979): a cylinder of unit height centered at $(x, y) = (70, 50)$ with base radius $15\Delta x$ containing a groove five zones wide. The width of the bridge connecting the two halves of the cylinder is ten zones. The initial condition and the numerical results for both schemes after one revolution are shown in Fig. 7. Several features are worth noting. As in the case before, Bott's scheme produces spurious oscillations as a result of large dispersion errors. The solution obtained with the combined scheme resembles the initial conditions quite well. However, the groove and the bridge are both eroded; that is, the discontinuities that were originally $1\Delta x$ wide are now smeared over several grid zones leading to a partial loss of the bridge connecting the two halves of the cylinder.

### c. *Deformational flow field test*

In this section the combined scheme was tested in the deformational flow field given by Smolarkiewicz (1982). The problem is the advection of a prescribed distribution [the same cone as in Fig. 5a superimposed upon a constant background value of $\psi_B = 100$ centered at $(x, y) = (50, 50)$] in a flow field defined by the streamfunction:

$$X(x, y) = 8 \sin\left(\frac{\pi x}{25}\right) \cos\left(\frac{\pi y}{25}\right). \tag{28}$$

The velocity components $(u, v)$ are given by

$$u = -\frac{\partial X}{\partial y}, \quad v = \frac{\partial X}{\partial x}. \tag{29}$$

Obviously, the given $X$ distribution yields a strong deformational flow field consisting of sets of symmetrical vortices, each vortex occupying a square with lateral lengths of 25 grid zones. As already mentioned by Smolarkiewicz (1982), this flow field could not be regarded as typical for atmospheric situations but it serves as a stringent test for the numerical stability of a numerical scheme.

Recently, Staniforth et al. (1987) presented the analytical solution of this problem. They pointed out that the length scale of the exact solution diminishes as a function of time. Hence, in the context of the evaluation of the performance of a numerical scheme it ap-

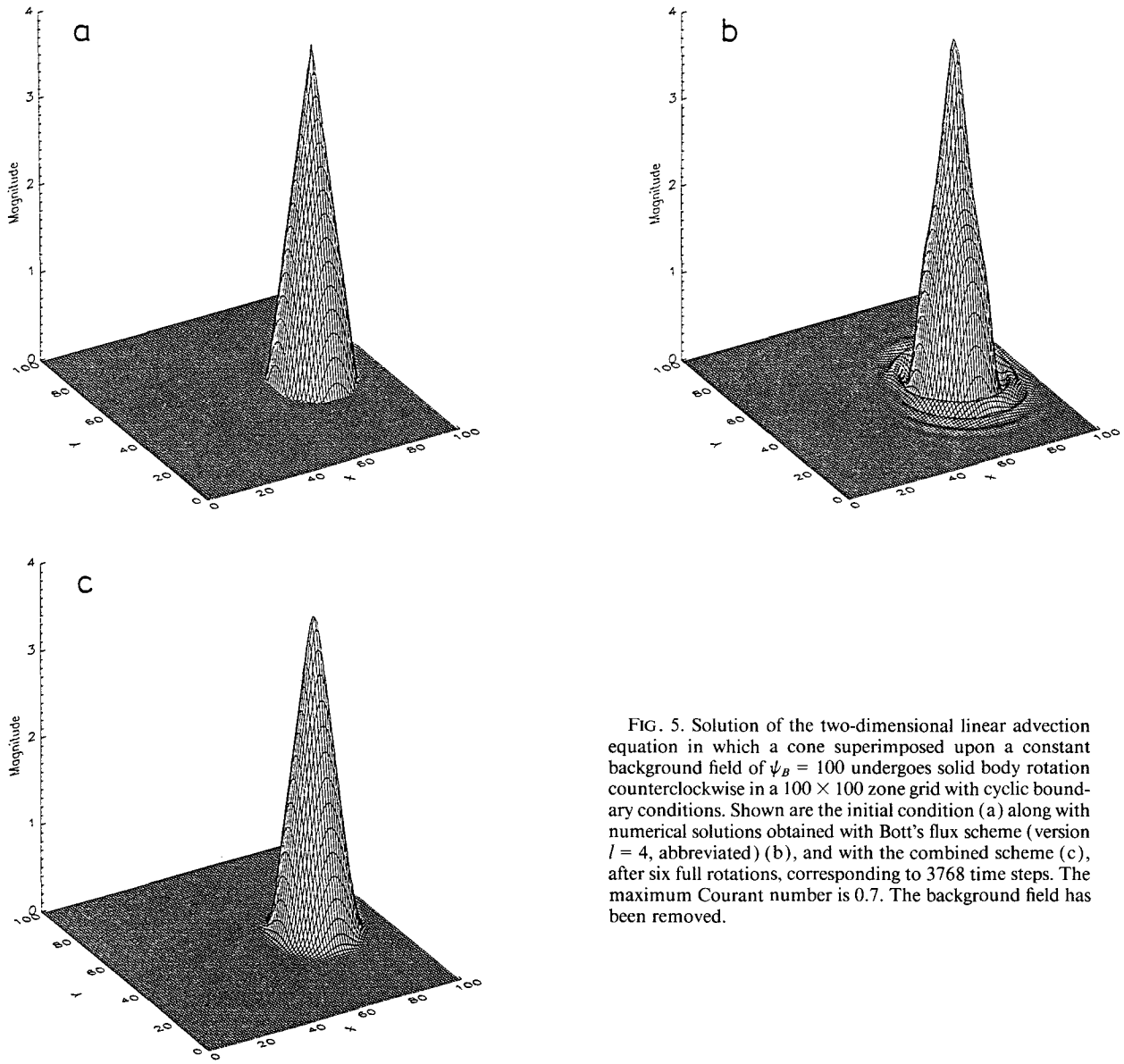


FIG. 5. Solution of the two-dimensional linear advection equation in which a cone superimposed upon a constant background field of $\psi_B = 100$ undergoes solid body rotation counterclockwise in a $100 \times 100$ zone grid with cyclic boundary conditions. Shown are the initial condition (a) along with numerical solutions obtained with Bott's flux scheme (version $l = 4$, abbreviated) (b), and with the combined scheme (c), after six full rotations, corresponding to 3768 time steps. The maximum Courant number is 0.7. The background field has been removed.

pears convenient to compare the numerical solution with the exact one only for short integration times in a quantitative manner, whereas for longer integration times the numerical scheme should be evaluated on the basis of stability.

Figures 8a–d depict the numerical short-term solutions (i.e., for integration periods, when the space scales of the analytical solution are still resolvable by the numerical grid mesh) obtained with the combined scheme with a time step of $\Delta t = 0.7$ after 19, 38, 57, and 75 iterations (background values removed). Since in the deformational flow field test Bott's scheme produces solutions that are very close to those obtained with the combined scheme [except that Bott's scheme yields little undershooting values (about 5% of the initial maximum) in the vicinity of sharp gradients], their presentation will be omitted here. The distributions calculated with the combined scheme quite closely resemble those of the analytical solution presented in Figs. 3a–d of Staniforth et al. (1987). After 19 steps, the numerical solution is almost indistinguishable from the exact one. As time evolves, the distribution inside each vortex spirals around the vortex center. As a result, the flow develops its strongest gradients at vortex boundaries, where the solution becomes almost vertical. After 38 and 57 iterations, the numerical solution quite closely matches that of the exact solution, although

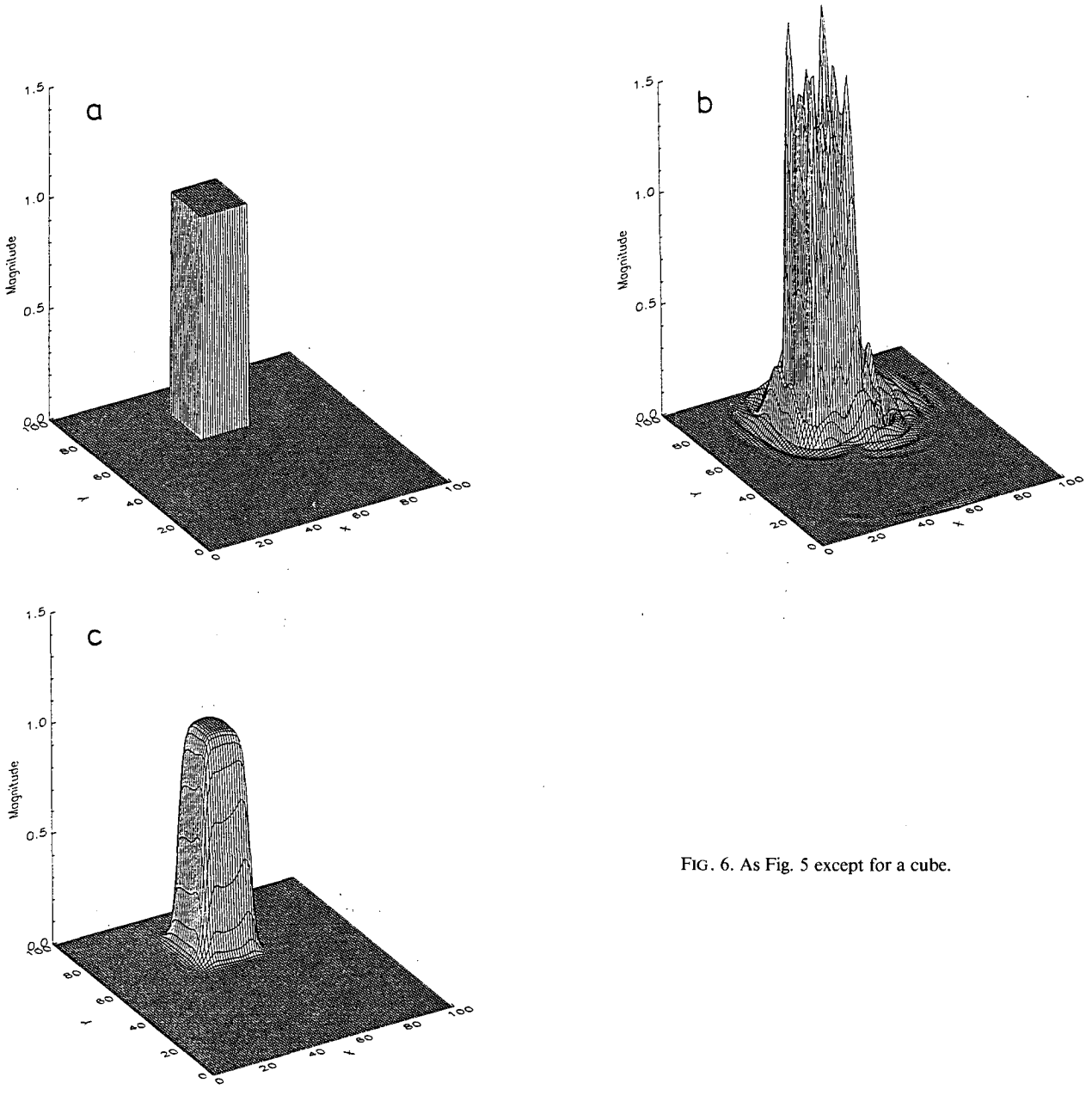


FIG. 6. As Fig. 5 except for a cube.

the gradients developing at the boundaries of each vortex are not as steep as in the exact solution. After 75 time steps, these gradients are nearly completely eroded at the upper boundaries of the central vortices. However, the numerical solution still faithfully represents the main features of the analytical solution; especially, it maintains the right–left symmetry as it should. Finally, we note that for long time-integration periods, which are beyond the limit at which any numerical method (which uses our mesh spacing) is capable of representing all space scales of the exact solution, the combined scheme generates no numerical instabilities but produces bounded solutions. This result differs from Bott (1989a), who reports that his long-term solution produces slight numerical instabilities.

To conclude the discussion of linear advection, one point is worth noting. We have demonstrated that the combined scheme performs quite well on linear advection problems and could be regarded as superior relative to Bott's scheme. However, this gain in accuracy must be weighted against computational costs.

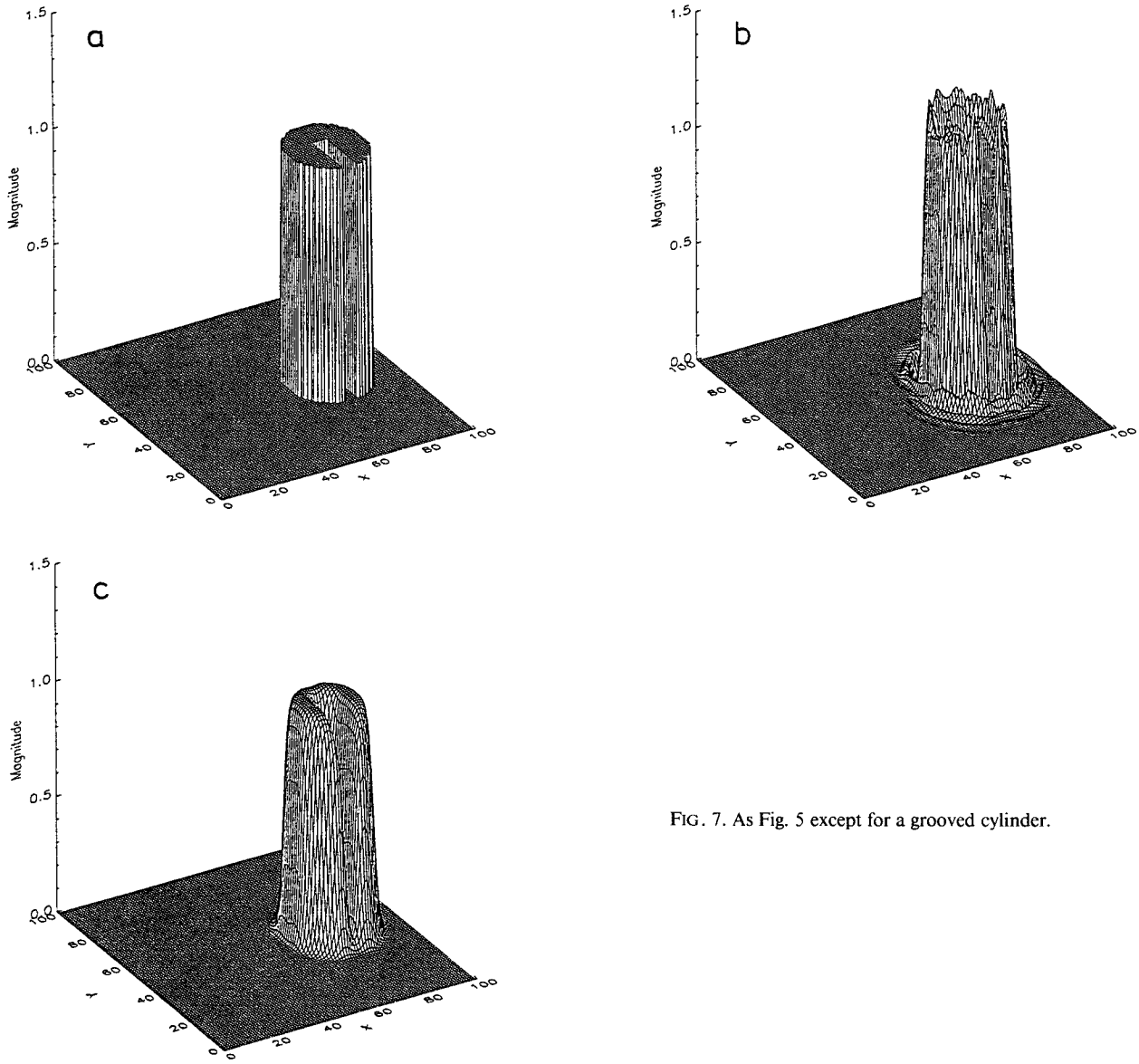


FIG. 7. As Fig. 5 except for a grooved cylinder.

This issue is addressed in Table 3 where we have listed CPU times of the combined scheme relative to Bott's scheme for the different test problems. Both schemes are completely vectorizably coded. It turns out that one has to pay only a relatively low price for the highly improved performance of the combined scheme. The combined scheme is less than twice as expensive as Bott's scheme. Since Bott's scheme requires about three times as much CPU time as the usual upstream scheme, the combined transport algorithm appears quite suitable for a large variety of applications in atmospheric modeling and thus gives a good balance between accuracy and efficiency.

## 4. Conclusions

A simple and effective self-adjusting hybrid technique has been introduced to construct a new conservative and monotonic advection scheme that is computationally very efficient. In principle, the scheme combines Bott's (1989a,b) area-preserving flux-form algorithm, which is used in smooth regions of the flow, with an area-preserving exponential interpolating scheme, which is used in regions where monotonicity might be violated (i.e., in regions of sharp gradients of the transported quantity). The use of either of these two schemes at any particular lo-

cation is controlled by a switch that—depending essentially on the local curvature of the advected variable—automatically switches from one scheme to the other. Since the exponential interpolation functions are monotonic by construction, no specific flux limiters have to be employed to avoid rippling.

Using a standard linear advection test, we evaluated the accuracy of the combined scheme relative to Bott's scheme. The comparative test calculations presented demonstrate the combined scheme's ability to accurately transport well-resolved, smoothly varying functions over large distances. Furthermore, the combined scheme is also well suited to address problems with sharp gradients, and returns solutions that are virtually as good as those predicted by Bott's scheme in respect to capturing steep gradients, but without the deficiency of the latter to produce physically unrealistic and often serious spurious oscillations. Taken together, the combined scheme is mass conservative, has excellent amplitude and phase characteristics, exhibits very low numerical diffusion of resolvable scales, obviates numer-

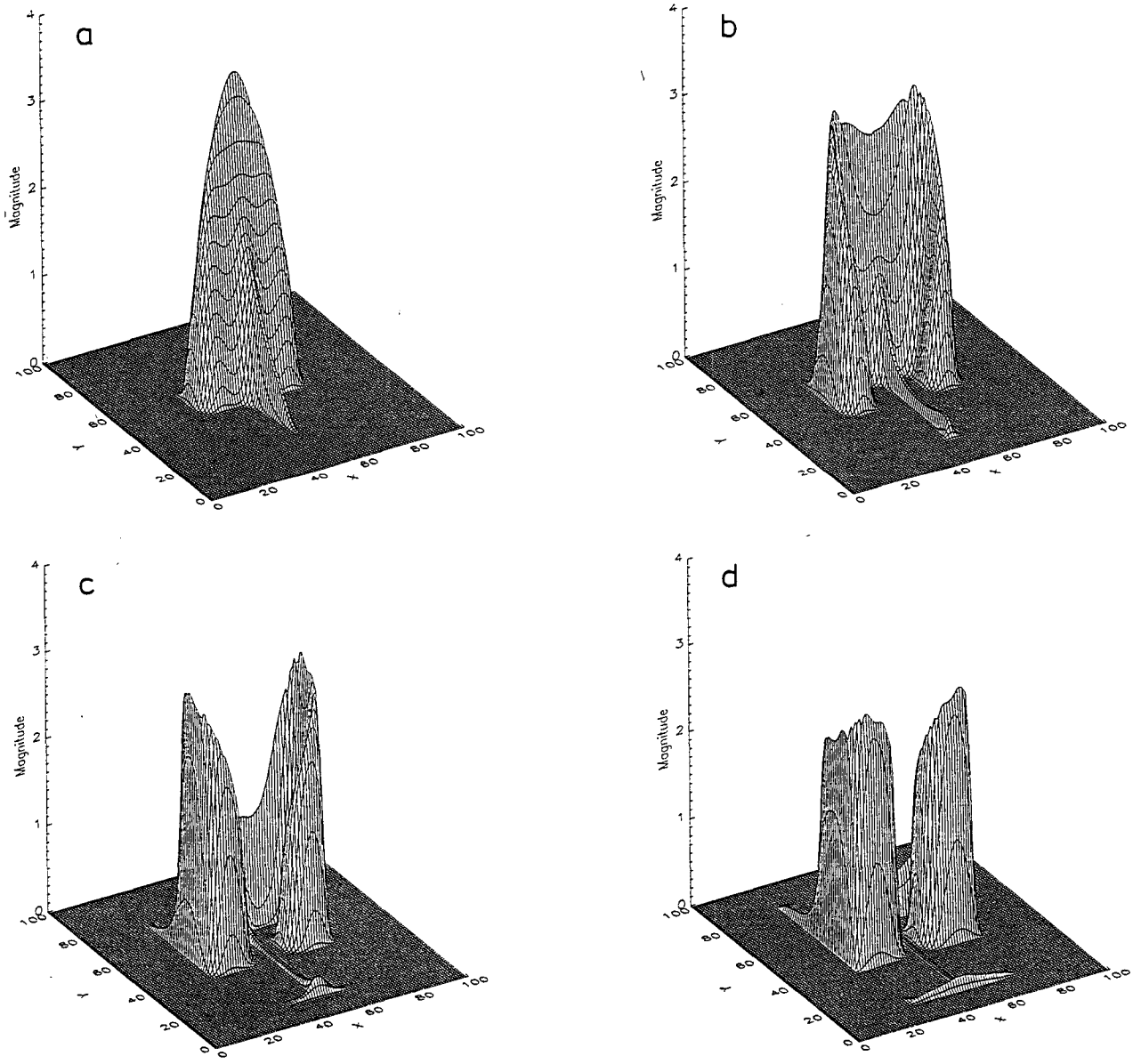


FIG. 8. Solution of the two-dimensional linear advection equation in which a cone centered on the center of a 100 × 100 point grid domain superimposed upon a constant background field of $\psi_B = 100$ is exposed in a deformational flow field. Shown are numerical results of the deformational flow field test obtained with the combined scheme with $\Delta t = 0.7$ after (a) 19, (b) 38, (c) 57, and (d) 75 iterations. The background field has been removed.

TABLE 3. CPU time requirements (on a CRAY 2S) for the combined scheme. CPU time is given relative to Bott's scheme (version $l = 4$, abbreviated) for different advection experiments after 3768 time steps.

| Test | Relative CPU time |
|---|---|
| Rotating cone | 1.61 |
| Rotating cube | 1.65 |
| Rotating cylinder | 1.72 |
| Deformational flow field | 2.03 |

ical artifacts such as dispersive ripples, and is numerically relatively inexpensive. Hence, it appears that the combined scheme is well suited for many atmospheric modeling applications, and its use is especially recommended for high-Reynolds number flows where advection plays a significant role to assure that numerical models reflect the physics of the system rather than the inaccuracies of the numerical methods.

*Acknowledgments.* The author wishes to thank Prof. Dr. H. Hinzpeter for his close interest in this study. Thanks also to Mrs. B. Zinecker for typing the manuscript.

## REFERENCES

Book, D. L., J. P. Boris, and K. Hain, 1975: Flux-corrected transport II: Generalizations of the method. *J. Comput. Phys.*, **18,** 248–283.

Boris, J. P., and D. L. Book, 1973: Flux corrected transport. I. SHASTA, A fluid transport algorithm that works. *J. Comput. Phys.*, **11,** 38–69.

——, and ——, 1976: Flux corrected transport III: Minimal error FCT algorithms. *J. Comput. Phys.*, **20,** 397–431.

Bott, A., 1989a: A positive definite advection scheme obtained by non-linear renormalization of the advective fluxes. *Mon. Wea. Rev.*, **117,** 1006–1015.

——, 1989b: Reply. *Mon. Wea. Rev.*, **117,** 2633–2636.

——, 1992: Monotone flux limitation in the area preserving flux form advection algorithm. *Mon. Wea. Rev.*, **120,** 2592–2602.

Carpenter, R. L., K. K. Droegemeier, P. R. Woodward, and C. E. Hane, 1990: Application of the piecewise parabolic method (PPM) to meteorological modeling. *Mon. Wea. Rev.*, **118,** 586–612.

Colella, P., and P. R. Woodward, 1984: The piecewise parabolic method (PPM) for gas-dynamical simulations. *J. Comput. Phys.*, **54,** 174–201.

Crowley, W. P., 1968: Numerical advection experiments. *Mon. Wea. Rev.*, **96,** 1–11.

Harten, A., and G. Zwas, 1972: Self-adjusting hybrid schemes for shock computations. *J. Comput. Phys.*, **9,** 568–583.

Lax, P. D., and B. Wendroff, 1960: Systems of conservation laws. *Commun. Pure Appl. Math.*, **13,** 217–237.

Müller, R., 1992: The performance of classical versus modern finite-volume advection schemes for atmospheric modeling in a one-dimensional test-bed. *Mon. Wea. Rev.*, **120,** 1407–1415.

Peyret, R., and T. D. Taylor, 1983: *Computational Methods for Fluid Flow.* Springer-Verlag, 358 pp.

Prather, M. J., 1986: Numerical advection by conservation of second-order moments. *J. Geophys. Res.*, **91,** 6671–6681.

Rood, R. B., 1987: Numerical advection algorithms and their role in atmospheric transport and chemistry models. *Rev. Geophys.*, **25,** 71–100.

Russel, G. L., and J. A. Lerner, 1981: A new finite-differencing scheme for the tracer transport equation. *J. Appl. Meteor.*, **20,** 1483–1498.

Smolarkiewicz, P. K., 1982: The multi-dimensional Crowley advection scheme. *Mon. Wea. Rev.*, **110,** 1968–1983.

——, 1983: A simple positive definite advection scheme with small implicit diffusion. *Mon. Wea. Rev.*, **111,** 479–486.

——, 1984: A fully multi-dimensional positive definite advection transport algorithm with small implicit diffusion. *J. Comput. Phys.*, **54,** 325–362.

——, and W. W. Grabowski, 1990: The multi-dimensional positive definite advection transport algorithm: Nonoscillatory option. *J. Comput. Phys.*, **86,** 355–375.

Spalding, D. B., 1972: A novel finite-difference formulation for differential expressions involving both first and second derivatives. *Int. J. Num. Methods Eng.*, **4,** 551.

Strang, G., 1968: On the construction and comparison of difference schemes. *SIAM. J. Num. Anal.*, **5,** 506–517.

Staniforth, A., J. Côté, and J. Pudykiewicz, 1987: Comments on "Smolarkiewicz's deformational flow." *Mon. Wea. Rev.*, **115,** 894–902.

Tremback, C. J., J. Powell, W. R. Cotton, and R. A. Pielke, 1987: The forward-in-time upstream advection scheme: Extension to higher orders. *Mon. Wea. Rev.*, **115,** 540–555.

Woodward, P. R., 1986: Piecewise parabolic methods for astrophysical fluid dynamics. *Astrophysical Radiation Hydrodynamics,* K.-H. Winkler and M. L. Norman, Eds., D. Reidel, 245–326.

——, and P. Colella, 1984: The numerical simulation of two-dimensional fluid flow with strong shocks. *J. Comput. Phys.*, **54,** 115–173.

Yanenko, N. N., 1971: *The Method of Fractional Steps.* Springer-Verlag, 160 pp.

Zalesak, S. T., 1979: Fully multi-dimensional flux-corrected transport for fluids. *J. Comput. Phys.*, **31,** 335–362.